Int J Clin Exp Med 2022;15(2):61-67
www.ijcem.com /ISSN:1940-5901/IJCEM0130415

Original Article

The value of intravoxel incoherent motion diffusion-weighted magnetic resonance imaging in the differential diagnosis of thyroid carcinoma and nodular goiter

Zhao Dong Ai[1], Xiao Ping Yu[1], Jing Hou[1], Jun Liu[1], Qiang Lu[1], Zhi Yuan Zhang[1], Jie Chen[2]

Departments of [1]Centre of Diagnostic Radiology, [2]Head and Neck Surgery, Hunan Cancer Hospital & The Affiliated Cancer Hospital of Xiangya School of Medicine, Central South University, Changsha 410013, Hunan, China

Received January 19, 2021; Accepted September 22, 2021; Epub February 15, 2022; Published February 28, 2022

Abstract: Purpose: To explore the differentiating diagnostic value of intravoxel incoherent motion diffusion-weighted magnetic resonance imaging (IVIM-DWI) in the diagnosis of thyroid carcinoma and thyroid nodular goiter. Methods: Thirty-two patients with thirty-nine thyroid nodules, underwent magnetic resonance imaging (MRI) examination including IVIM-DWI sequencing before their operations. Differences in standard apparent diffusion coefficient (ADC_S), slow apparent diffusion coefficient (D), fast apparent diffusion coefficient (D*) and fraction of fast apparent diffusion coefficient (*f*) values between the thyroid carcinoma group and nodular goiter group were compared. Parameters such as receiver operating characteristic (ROC) curves, diagnostic thresholds and diagnostic performance were obtained. Results: The values of ADC_S and D in the thyroid carcinoma group were distinctly smaller than those in the nodular goiter group. The value of D* from the thyroid carcinoma group was higher than that from the nodular goiter group, but the value of *f* was lower than that of the nodular goiter group, although not significantly. In the differentiation of the thyroid carcinoma group from the nodular goiter group, the area under the curve (AUC), sensitivity, specificity and threshold values were 0.825, 100%, 57.9%, and 1.31×10^{-3} mm^2/s respectively for ADC_S and 0.849, 95%, 63.2%, and 0.856×10^{-3} mm^2/s for D. Conclusion: ADC_S and D were valuable for differentiating between thyroid carcinoma and nodular goiter.

Keywords: Thyroid nodule, intravoxel incoherent motion, diffusion-weighted imaging, apparent diffusion coefficient, pathology, differential diagnosis

Introduction

The incidence of thyroid nodules has increased significantly in recent years, and thyroid cancer in thyroid nodules is found in 5% to 10% of these cases [1, 2]. The treatment regimens of benign and malignant thyroid nodules are quite different, so early differentiation of malignant nodules from benign nodules is very important.

Conventional magnetic resonance diffusion-weighted imaging (DWI) is valuable for distinguishing malignant thyroid nodules from benign thyroid nodules [3, 4]. Studies on conventional DWI have shown that the apparent diffusion coefficient (ADC) values of malignant thyroid nodules are smaller than those of benign thyroid nodules [5-9]. However, Schueller-Weidekamm obtained contradictory results. It is difficult to give a reasonable explanation for these contradictory results [10, 11]. The findings might be partly due to the conventional DWI, which is based on a mono-exponential model that ignores the effect of microcirculation perfusion on the signal intensity of DWI. Le Bihan proposed intravoxel incoherent motion (IVIM) theory and conducted a series of studies [12-15].

Magnetic resonance intravoxel incoherent motion diffusion weighted imaging (IVIM-DWI), which is founded on a double exponential model, can separate the diffusion of water mol-

ecules from microcirculation perfusion, providing more information for diagnosis. There are few studies reporting on the value of IVIM-DWI in distinguishing malignant and benign thyroid nodules. Thyroid carcinoma is the most common malignant nodule of the thyroid. Locally, nodular goiter is the most common benign thyroid nodule. Clinically, in our hospital, thyroid cancer accounts for more than 90% of the malignant thyroid nodules, and nodular goiters account for approximately 85% of the benign thyroid nodules. In this study, we used IVIM-DWI to conduct a preliminary study of thyroid nodules to explore its value in distinguishing thyroid carcinoma from thyroid nodular goiters.

Methods

Patient selection

Approval of the retrospective project was obtained from the Ethics Committee of our hospital (approval number: 2019-169), and all patients gave informed consent. Inclusion criteria were as follows: 1. Short lesion diameter greater than 8 mm; 2. Solid nodule or priority to solid; 3. Nodules scheduled for surgical resection; and 4. Patient older than 18 years. Exclusion criteria were as follows: 1. Patient refused to join the experiment; 2. Patient had contraindications for MRI; and 3. Cystic nodule or priority to cystic. All patients received ultrasound examination, and the sonographer considered the nodule to be Ti-RADS level 4 or 5. Computed tomography (CT) and MRI examinations were performed before the operation. The postoperative pathological examination confirmed the characteristics of the nodule.

Conventional MRI protocol

All patients were examined by a 1.5-Tesla MRI machine (Optima MR360; GE Healthcare, USA) with a combined head and neck coil. Imaging protocol included: 1) cross sectional T1-weighted spin-echo sequence, repetition time (TR)/echo time (TE) was 499/8.5 milliseconds, number of excitation (NEX) =4; 3 mm (millimeter) slice thickness, 1 mm slice gap; 2) cross sectional T2-weighted spin-echo sequence with fat saturated, TR/TE was 3296/84 milliseconds; 3 mm section thickness, 1 mm intersection gap; NEX=4. Acquisition matrix 288×192, field of view (FOV) 24 cm×19.2 cm (centimeter). The routine scan ranged from the hyoid bone to the upper margin of the sternum.

IVIM-DWI protocol

A single-shot diffusion-weighted spin-echo echo-planar sequence with twelve *b* values was applied, which was 0, 10, 20, 30, 50, 80, 100, 150, 200, 400, 600 and 800 s/mm^2. Scanning parameters: TR/TE was 4072/88.9 milliseconds, FOV 22 cm×18 cm, gathering matrix 128×128, slice thickness was 3 mm, slice gap was 1 mm, NEX=4. The IVIM scan range was determined by the size and location of the lesions shown in the conventional sequence.

IVIM-DWI analysis

All IVIM-DWI data were processed by FuncTool software (version AW 4.6, GE medical system) attached to the Advantage Workstation. Two radiologists assessed the data independently and were double-blinded to the pathological results of all thyroid lesions. These radiologists had more than ten years' experience in the field of head and neck radiology. The main principles and processes of IVIM-DWI analysis have been described previously [16-18]. According to the formula $S_b/S_0 = (1\text{-}f) \exp(-b\ D) + f \exp(-b\ D^*)$, S_b is the signal strength when the diffusion sensitivity coefficient b-value is greater than 0 s/mm^2, S_0 is the signal strength with a b-value of 0 s/mm^2, D represents the real diffusion coefficient with the pure diffusion of the water molecules in tissue, D* represents the pseudo diffusion coefficient associated with microcirculation perfusion, and *f* represents the fraction of microvascular volume. The ADC_S value was generated with the conventional DWI formula $S_b/S_0 = \exp(-b\ D)$, where the MRI data had higher b-values (200, 400, 600, 800 s/mm^2).

The regions of interest (ROI) with thyroid nodule parenchyma were drawn manually on the largest cross-section level, avoiding cystic, bleeding, necrosis and calcification areas on IVIM-DWI parametric maps. Axial T1-weighted, T2-weighted imaging and computed tomography imaging were used as references. The area of the ROI was 58-711 mm^2, continuous measurement was performed three times and the average taken, and the value of ADC_S, D (slow ADC),

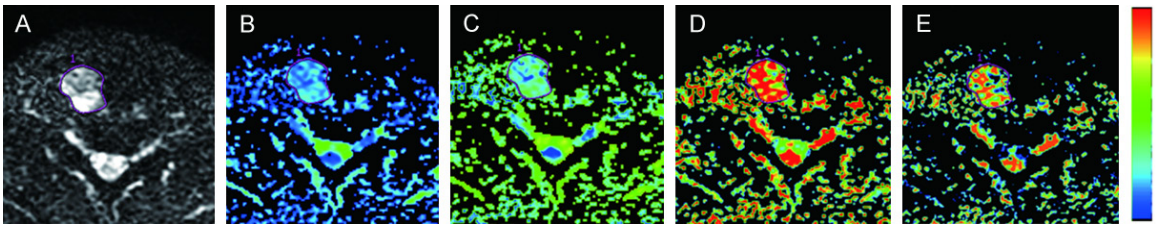

Figure 1. (A-E) Sixty-year old man, thyroid papillary carcinoma. Transverse IVIM image when b value was zero (A). Transverse pseudocolorized images for ADC_S (B), D (C), D* (D), and *f* (E).

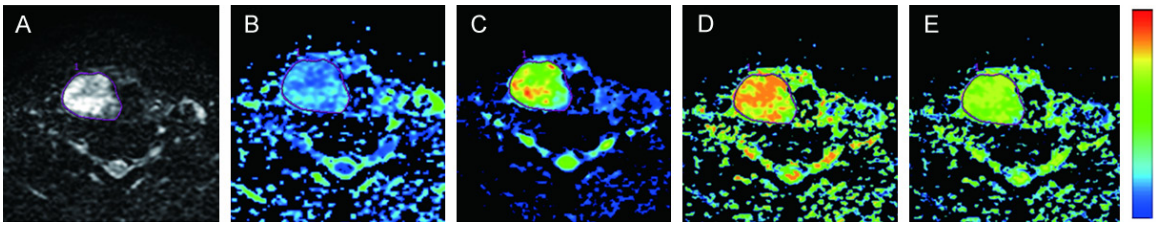

Figure 2. (A-E) Forty-eight-year old female, nodular goiter, transverse IVIM image when the b value was zero (A). Transverse pseudocolorized images for ADC_S (B), D (C), D* (D), and *f* (E).

D* (fast ADC) and *f* (fraction of fast ADC) were obtained, and pseudo-color map. The final value for each nodule was the average of the initial value from the two observations.

Statistical analysis

Statistical methods SPSS 19.0 software (SPSS Inc., Chicago, Ill) was used. The values with the IVIM-DWI parameters of thyroid carcinoma and nodular goiter are described as the mean ± standard deviation. The values of the IVIM-DWI parameters between the two groups were compared with the Mann-Whitney U test. The optimal diagnostic threshold was obtained by plotting the receiver operating characteristic (ROC) curve, and the diagnostic efficiency for each parameter was contrasted by the area under the curve (AUC). The AUCs of the ADC_S and D were compared using the Z test (software MedCalc 17.6). $P<0.05$ was considered statistically significant.

Results

Consecutive patients with thyroid nodules were enrolled from January to June 2019 in our hospital. The study included 37 patients, but 5 patients were removed because of poor imaging. The final sample consisted of the remaining 32 patients, which included 5 males and 27 females, ages 18 to 65 years old. The mean ages of patients with nodular goiter and thyroid carcinoma were 39.1±14.79 years old and 45.95±10.89 years old, respectively. No distinct difference in age was observed between the two groups (P=0.12). Thirty-nine thyroid nodules were included, of which 20 were nodular goiters and 19 were thyroid carcinomas (papillary carcinoma 18, undifferentiated carcinoma 1). The conventional MRI sequence images clearly showed 39 lesions, and the short diameter of lesions was greater than 8 mm (**Figures 1** and **2**).

The parameter values of IVIM-DWI for the thyroid carcinoma and nodular goiter group are summarized in **Table 1**. The values of ADC_S and D in with the thyroid carcinoma group were remarkably lower than those in the nodular goiter group. The value of D* in the thyroid carcinoma group was higher than that in the nodular goiter group, and the value of *f* was lower than that of the nodular goiter group, although not significantly. There were color differences between the two groups on the pseudocolor graphs of the IVIM parameters (**Figures 1B-E** and **2B-E**). There was no significant difference in the area under the ROC curves between the ADC_S and D values (P=0.727).

The values of the IVIM-DWI correlation index (AUC, sensitivity, specificity and Youden index) are shown in **Table 2**. ROC curve is shown in

Table 1. IVIM parameters of thyroid carcinoma and nodular goiter

IVIM-DWI	Nodular goiter group	Thyroid carcinoma group	*P* value
ADC_S ($\times10^{-3}$ mm^2/s)	1.82±0.41	1.24±0.43	<0.001
D ($\times10^{-3}$ mm^2/s)	1.39±0.44	0.81±0.39	<0.001
D* ($\times10^{-3}$ mm^2/s)	91.92±37.84	102.40±72.04	0.813
f (fraction of D*) (%)	31.68±8.92	28.80±9.48	0.247

IVIM-DWI, intravoxel incoherent motion diffusion-weighted magnetic resonance imaging; ADC_S, standard ADC; D, slow ADC; D*, fast ADC; *f*, fraction of fast ADC.

Table 2. Diagnostic performance of each IVIM parameter with nodular goiter

IVIM-DWI	AUC	Youden index	Sensitivity (%)	Specificity (%)
ADC_S	0.825	0.579	100	57.9
D	0.849	0.582	95	63.2
D*	0.522	0.271	85	42.1
f	0.609	0.282	65	63.2

IVIM-DWI, intravoxel incoherent motion diffusion-weighted magnetic resonance imaging; ADC_S, standard apparent diffusion coefficient; D, slow ADC; D*, fast ADC; *f*, fraction of fast ADC; AUC, area under the curve of receiver operating characteristic curve.

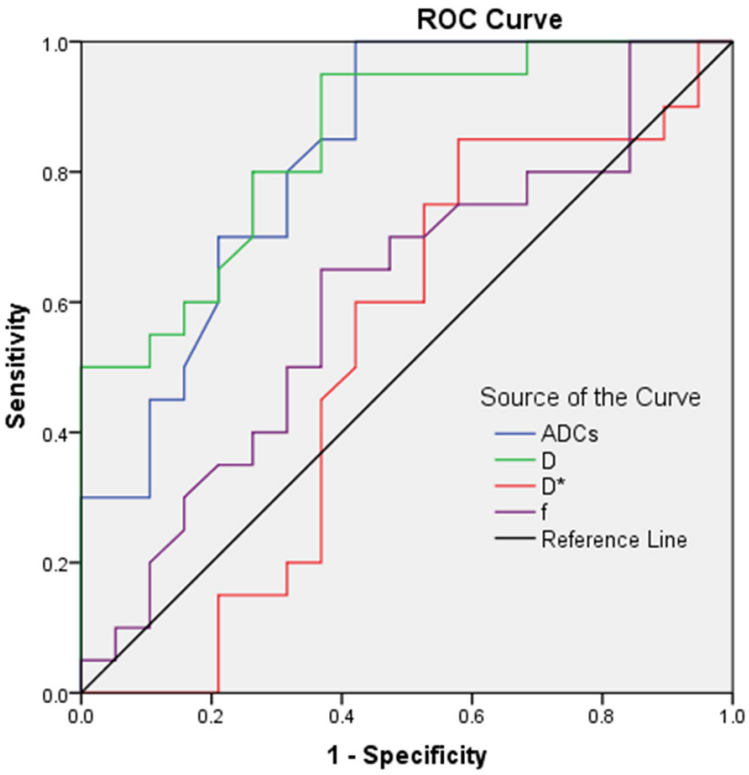

Figure 3. Receiver operating characteristic curves for the ADC_S, D, D*, *f*.

Figure 3. The optimal cutoff values of the ADC_S and D are 1.31×10^{-3} mm^2/s and 0.856×10^{-3} mm^2/s, respectively. D had the highest specificity and the highest AUC, and ADC_S had the highest sensitivity among all the IVIM-based parameters.

Discussion

Our research revealed that IVIM-DWI has the potential ability to distinguish thyroid carcinoma from nodular goiter, and the diagnostic efficiency of D is similar to that of ADC_S.

Our data showed that the values of ADC_S and D with thyroid carcinoma were significantly lower than those of nodular goiter, which was consistent with most studies of conventional DWI [3-9]. D is determined mainly by the density of cells along with the component of extracellular matrix [19-22]. It is widely believed that ADC_S value and D value are negatively correlated with tissue cell density, as is the nucleus-to-cytoplasm ratio [20-23]. We think the thyroid carcinoma had higher cell density, higher nucleus-to-cytoplasm ratio, water molecule diffusion was limited and had lower ADC_S and D values. The AUC of D was slightly higher than the AUC of ADC_S but not statistically significant, which implied that the diagnostic performance of D was similar to that of ADC_S. In accordance with the IVIM theory, D presents the true diffusion coefficient of tissue which was caused by water molecule Brownian movement, and D* presents the pseudo diffusion coefficient of tissue caused by microcirculation perfusion. ADC_S reflect total diffusion, including D and D*. No distinct difference in D* was observed between the two groups, so the ADC_S and D have the same direction between the two groups.

However, some studies believe that D is better than ADC_S in differentiating malignant and benign tumor tissue, as in breast tumors [24-26], prostate cancer and benign prostate tissue [27, 28], and benign and malignant hepatic tumors [29, 30]. Woo Sungmin found that both the D and ADC_S values were distinctly negatively related to the histological grade of hepatocellular carcinoma (HCC). In the process of distinguishing high-level HCC from low-level HCC, the D value was remarkably superior to the ADC value [31]. Yu-Dong Zhang obtained similar results with D, ADC_S value and pathological grades in prostate cancer; the D value performed better than the ADC_S value in differentiating low-level prostate carcinoma from medium/high-level prostate carcinoma [32]. Perhaps the differences in organizational structure lead to the different results.

In our study, the value of the *f* with thyroid carcinoma group was slightly lower than that of the nodular goiter group, and the D* value of the thyroid carcinoma group slightly exceeded the value of the nodular goiter group, with no significant difference ($P \geq 0.247$). *F* and D* are indicators related to perfusion, reflecting the blood volume and average blood flow velocity of the microvasculature, respectively [17, 18]. We suggest that the blood volume of a nodular goiter is slightly higher than that of thyroid carcinoma, the blood flow velocity with a nodular goiter is slightly slower than that of thyroid carcinoma, and the difference in blood flow capacity is not significant. Similarly, Ben-David found that the difference between the quantitative and semiquantitative perfusion parameters of benign and malignant nodules was not significant [33]. Our results are inconsistent with Tan's results [34]. We need to expand the sample size for further research. Future studies about the correlation between D*, *f* and perfusion parameters are needed.

Our study has some limitations. First, the sample size was small, which may result in statistical bias. Second, the values of the parameters with smaller nodules (the short diameter <8 mm) were removed due to the partial volume effect. Third, the heterogeneity of the lesion affects the accuracy of the parameter measured, such as microcalcification, tiny cystic change, and micronecrosis. Fourth, because the ROI were manually sketched, error was difficult to avoid. Finally, a few cases were removed because of poor image quality or vascular pulse artifacts, and the scanning sequence needed to be improved to reduce artifacts and improve image quality.

In conclusion, our data showed that ADC_S and D were valuable for differentiating between thyroid carcinoma and nodular goiter, and the differential diagnostic efficacy was similar.

Acknowledgements

This study was supported by the Special Fund for Tumor Research at the National Cancer Center (China) (No. NCC2017A19).

Disclosure of conflict of interest

None.

Address correspondence to: Dr. Xiao Ping Yu, Department of Centre of Diagnostic Radiology, Hunan Cancer Hospital & The Affiliated Cancer Hospital of Xiangya School of Medicine, Central South University, 283 Tongzipo Road, Yuelu District, Changsha 410013, Hunan, China. Tel: +86-13607313419; Fax: +86-731-89762577; E-mail: nj9015@163.com

References

[1] Bomeli SR, Lebeau SO and Ferris RL. Evaluation of a thyroid nodule. Otolaryngol Clin North Am 2010; 43: 229-238.

[2] Sharen G, Zhang B, Zhao R, Sun J, Gai X and Lou H. Retrospective epidemiological study of thyroid nodules by ultrasound in asymptomatic subjects. Chin Med J (Engl) 2014; 127: 1661-1665.

[3] Mutlu H, Sivrioglu AK, Sonmez G, Velioglu M, Sildiroglu HO, Basekim CC and Kizilkaya E. Role of apparent diffusion coefficient values and diffusion-weighted magnetic resonance imaging in differentiation between benign and malignant thyroid nodules. Clin Imaging 2012; 36: 1-7.

[4] Bozgeyik Z, Coskun S, Dagli AF, Ozkan Y, Sahpaz F and Ogur E. Diffusion-weighted MR imaging of thyroid nodules. Neuroradiology 2009; 51: 193-198.

[5] Aydın H, Kızılgöz V, Tatar İ, Damar Ç, Güzel H, Hekimoğlu B and Delibaşı T. The role of proton MR spectroscopy and apparent diffusion coefficient values in the diagnosis of malignant thyroid nodules: preliminary results. Clin Imaging 2012; 36: 323-330.

[6] Shi HF, Feng Q, Qiang JW, Li RK, Wang L and Yu JP. Utility of diffusion-weighted imaging in dif-

ferentiating malignant from benign thyroid nodules with magnetic resonance imaging and pathologic correlation. J Comput Assist Tomogr 2013; 37: 505-510.
[7] Brown AM, Nagala S, McLean MA, Lu Y, Scoffings D, Apte A, Gonen M, Stambuk HE, Shaha AR, Tuttle RM, Deasy JO, Priest AN, Jani P, Shukla-Dave A and Griffiths J. Multi-institutional validation of a novel textural analysis tool for preoperative stratification of suspected thyroid tumors on diffusion-weighted MRI. Magn Reson Med 2016; 75: 1708-1716.
[8] Vermoolen MA, Kwee TC and Nievelstein RA. Apparent diffusion coefficient measurements in the differentiation between benign and malignant lesions: a systematic review. Insights Imaging 2012; 3: 395-409.
[9] Chen L, Xu J, Bao J, Huang X, Hu X, Xia Y and Wang J. Diffusion-weighted MRI in differentiatin malignant from benign thyroid nodules: a meta-analysis. BMJ Open 2016; 6: e008413.
[10] Schueller-Weidekamm C, Schueller G, Kaserer K, Scheuba C, Ringl H, Weber M, Czerny C and Herneth AM. Diagnostic value of sonography, ultrasound-guided fine-needle aspiration cytology, and diffusion-weighted MRI in the characterization of cold thyroid nodules. Eur J Radiol 2010; 73: 538-544.
[11] Schueller-Weidekamm C, Kaserer K, Schueller G, Scheuba C, Ringl H, Weber M, Czerny C and Herneth AM. Can quantitative diffusion-weighted MR imaging differentiate benign from malignant cold thyroid nodules? Initial results in 25 patients. AJNR Am J Neuroradiol 2009; 30: 417-422.
[12] Le Bihan D, Breton E, Lallemand D, Aubin ML, Vignaud J and Laval-Jeantet M. Separation of diffusion and perfusion in intravoxel incoherent motion MR imaging. Radiology 1988; 168: 497-505.
[13] Le Bihan D and Turner R. The capillary network: a link between IVIM and classical perfusion. Magn Reson Med 1992; 27: 171-178.
[14] Le Bihan D. Intravoxel incoherent motion perfusion MR imaging: a wake-up call. Radiology 2008; 249: 748-752.
[15] Iima M and Le Bihan D. Clinical intravoxel incoherent motion and diffusion MR imaging: past, present, and future. Radiology 2016; 278: 13-32.
[16] Yu XP, Wen L, Hou J, Bi F, Hu P, Wang H and Wang W. Discrimination between metastatic and nonmetastatic mesorectal lymph nodes in rectal cancer using intravoxel incoherent motion diffusion-weighted magnetic resonance imaging. Acad Radiol 2016; 23: 479-485.
[17] Lu W, Jing H, Ju-Mei Z, Shao-Lin N, Fang C, Xiao-Ping Y, Qiang L, Biao Z, Su-Yu Z and Ying H. Intravoxel incoherent motion diffusion-weighted imaging for discriminating the pathological response to neoadjuvant chemoradiotherapy in locally advanced rectal cancer. Sci Rep 2017; 7: 8496.
[18] Li FP, Wang H, Hou J, Tang J, Lu Q, Wang LL and Yu XP. Utility of intravoxel incoherent motion diffusion-weighted imaging in predicting early response to concurrent chemoradiotherapy in oesophageal squamous cell carcinoma. Clin Radiol 2018; 73: 756, e17-26.
[19] Shim WH, Kim HS, Choi CG and Kim SJ. Comparison of apparent diffusion coefficient and intravoxel incoherent motion for differentiating among glioblastoma, metastasis, and lymphoma focusing on diffusion-related parameter. PLoS One 2015; 10: e0134761.
[20] Gloria C, Li Q, Xu L and Zhang W. Differentiation of diffusion coefficients to distinguish malignant and benign tumor. J Xray Sci Technol 2010; 18: 235-249.
[21] Fong D, Bhatia KS, Yeung D and King AD. Diagnostic accuracy of diffusion-weighted MR imaging for nasopharyngeal carcinoma, head and neck lymphoma and squamous cell carcinoma at the primary site. Oral Oncol 2010; 46: 603-606.
[22] Zhang SX, Jia QJ, Zhang ZP, Liang CH, Chen WB, Qiu QH and Li H. Intravoxel incoherent motion MRI: emerging applications for nasopharyngeal carcinoma at the primary site. Eur Radiol 2014; 24: 1998-2004.
[23] Jenkinson MD, du Plessis DG, Smith TS, Brodbelt AR, Joyce KA and Walker C. Cellularity and apparent diffusion coefficient in oligodendroglial tumours characterized by genotype. J Neurooncol 2010; 96: 385-392.
[24] Iima M, Yano K, Kataoka M, Umehana M, Murata K, Kanao S, Togashi K and Le Bihan D. Quantitative non-Gaussian diffusion and intravoxel incoherent motion magnetic resonance imaging: differentiation of malignant and benign breast lesions. Invest Radiol 2015; 50: 205-211.
[25] Liu C, Liang C, Liu Z, Zhang S and Huang B. Intravoxel incoherent motion (IVIM) in evaluation of breast lesions: comparison with conventional DWI. Eur J Radiol 2013; 82: e782-789.
[26] Bokacheva L, Kaplan JB, Giri DD, Patil S, Gnanasigamani M, Nyman CG, Deasy JO, Morris EA and Thakur SB. Intravoxel incoherent motion diffusion-weighted MRI at 3.0 T differentiates malignant breast lesions from benign lesions and breast parenchyma. J Magn Reson Imaging 2014; 40: 813-823.
[27] Shinmoto H, Tamura C, Soga S, Shiomi E, Yoshihara N, Kaji T and Mulkern RV. An intravoxel incoherent motion diffusion-weighted imaging study of prostate cancer. AJR Am J Roentgenol 2012; 199: W496-500.

[28] Döpfert J, Lemke A, Weidner A and Schad LR. Investigation of prostate cancer using diffusion-weighted intravoxel incoherent motion imaging. Magn Reson Imaging 2011; 29: 1053-1058.
[29] Yoon JH, Lee JM, Yu MH, Kiefer B, Han JK and Choi BI. Evaluation of hepatic focal lesions using diffusion-weighted MR imaging: comparison of apparent diffusion coefficient and intravoxel incoherent motion-derived parameters. J Magn Reson Imaging 2014; 39: 276-285.
[30] Luo M, Zhang L, Jiang XH and Zhang WD. Intravoxel incoherent motion diffusion-weighted imaging: evaluation of the differentiation of solid hepatic lesions. Transl Oncol 2017; 10: 831-838.
[31] Woo S, Lee JM, Yoon JH, Joo I, Han JK and Choi BI. Intravoxel incoherent motion diffusion-weighted MR imaging of hepatocellular carcinoma: correlation with enhancement degree and histologic grade. Radiology 2014; 270: 758-767.
[32] Zhang YD, Wang Q, Wu CJ, Wang XN, Zhang J, Liu H, Liu XS and Shi HB. The histogram analysis of diffusion-weighted intravoxel incoherent motion (IVIM) imaging for differentiating the gleason grade of prostate cancer. Eur Radiol 2015; 25: 994-1004.
[33] Ben-David E, Sadeghi N, Rezaei MK, Muradyan N, Brown D, Joshi A and Taheri MR. Semiquantitative and quantitative analyses of dynamic contrast-enhanced magnetic resonance imaging of thyroid nodules. J Comput Assist Tomogr 2015; 39: 855-859.
[34] Tan H, Chen J, Zhao YL, Liu JH, Zhang L, Liu CS and Huang D. Feasibility of intravoxel incoherent motion for differentiating benign and malignant thyroid nodules. Acad Radiol 2019; 26: 147-153.